Mathematical Biosciences and Engineering

MBE, 22 (9): 2391–2408.
DOI: 10.3934/mbe.2025087
Received: 05 February 2025
Revised: 29 June 2025
Accepted: 09 July 2025
Published: 22 July 2025

https://www.aimspress.com/journal/MBE

Research article

Unveiling environmental drivers of Moso bamboo sap flow using causal inference

Pengfei Deng and Zhaohui Jiang*

School of Information and Artificial Intelligence, Anhui Agricultural University, Hefei 230036, China

* **Correspondence:** Email: jiangzh@ahau.edu.cn.

Abstract: Studying the relationship between Moso bamboo sap flow and environmental factors is essential for understanding the water transpiration patterns of this species. Traditional methods often rely on correlation analysis, but correlation does not imply causation. To elucidate the underlying mechanisms of how major environmental factors influence Moso bamboo sap flow, we analyzed the causality between them. First, the Fast Causal Inference algorithm was used to explore non-temporal causal relationships. Subsequently, the Latent Peter-Clark Momentary Conditional Independence algorithm was employed to further analyze the temporal causal effects. We found causal relationships among factors with low gray correlation coefficients. Besides, illumination, air, and soil temperature promote the density increase of sap flow, while carbon dioxide concentration, air humidity, and soil temperature inhibit bamboo sap flow density overall. Among these factors, illumination exhibits the longest lagged causal effect approximately around 80 minutes, whereas carbon dioxide concentration and soil humidity can quickly affect the sap flow density, with approximately 20 minutes. The study presents a novel methodological approach to analyze the complex interplay between environmental factors and sap flow, providing a more explanatory and logical framework. This study offers a novel methodological framework for disentangling the complex interactions between environmental variables and sap flow, providing deeper insights into the dynamic processes driving Moso bamboo water use. The findings contribute to advancing plant physiology and environmental science, while opening avenues for future research in related fields.

Keywords: Moso bamboo; sap flow, environmental factors; causal inference; temporal observation; structural causal model

1. Introduction

Bamboo forests are widely recognized as a sustainable and renewable resource, often referred to as the "green gold" of the plant kingdom [1]. They play a significant role in regional soil erosion control and soil conservation [2]. Sap flow in plants reflects the dynamics of internal water transport, the characteristics of water utilization, and their responses to environmental changes [3]. Sap flow effectively transports essential soil nutrients, such as nitrogen, phosphorus, and potassium, to various parts of the plant, supporting its growth, development, and metabolic activities [4]. Additionally, it facilitates the distribution and transport of carbohydrates and other metabolites produced through photosynthesis within the plant, meeting the demands for growth and sustaining life processes [5].

Therefore, sap flow becomes one of the key indicators for analyzing plant water consumption characteristics and studying the mechanisms of plant water transport [6]. Zhu [7] investigated the relationship between the sap flow of Masson pine trunks and environmental factors. They employed Pearson correlation analysis and found that with the intensification of solar radiation and increased transpiration, the sap flow rate gradually increased. Li [8] primarily analyzed the correlation between sap flow in Chinese fir trunks and soil moisture. They utilized the Varimax rotation method to output score factors to assess the relationships between different factors. The study revealed that soil drought significantly inhibited daytime sap flow in Chinese fir. Tong [9] simulated summer drought conditions and found that sap flow density responded positively to solar radiation, vapor pressure deficit, and soil moisture, identifying them as key influencing factors. Fan [10], using the heat ratio method on pear trees, observed significantly higher sap flow during the day than at night, with vapor pressure and photosynthetically active radiation being key daytime drivers, and vapor pressure and plant water potential dominating at night. Due to the hollow structure of Moso bamboo, measuring sap flow is relatively challenging, and there are fewer related studies. Moreover, sap flow rate in Moso bamboo is mainly inferred by externally heating the bamboo or using light pulses and observing corresponding temperature changes. Hou [11] utilized the Dynamax sap flow measurement system to monitor the diurnal variation of sap flow in Moso bamboo within the Zhejiang Miaoshanwu Natural Reserve. Through Pearson correlation analysis and multiple linear regression analysis, they investigated the relationship between sap flow and environmental factors and established a regression model. The researchers found that on sunny days, the variation of sap flow exhibited a unimodal curve, showing significant changes. Conversely, on overcast or rainy days, the curve appeared bimodal or multimodal, with daily average sap flow rate and sap flow volume lower than those on sunny days, exhibiting a more gradual change. Additionally, correlation analysis revealed that sap flow rate was significantly positively correlated with air temperature, photosynthetically active radiation, total radiation, and vapor pressure deficit (correlation coefficients often exceeding 0.85), while it was significantly negatively correlated with relative humidity. Gu [12] compared the sensitivity of transpiration in Moso bamboo of different ages and phenological periods to environmental variables. Using SPSS avr13.0 software for statistical correlation analysis of various variables, the study revealed that with the increase in solar radiation from spring to summer, the daily cumulative sap flow density exhibited an upward trend. Additionally, the older the bamboo, the later the daily sap flow peak occurred, and the lower the daily cumulative sap flow amount was. Liu [13] investigated seasonal variations in sap flow rates of Moso bamboo. Through visual analysis of the data, they found that solar radiation was the dominant factor influencing sap flow during spring and summer, while the vapor pressure deficit became the primary influencing factor in autumn and winter. Wu [14] discovered that drought led to

reductions in both transpiration and growth of Moso bamboo. The underlying cause was a decrease in stomatal conductance. However, the addition of a certain amount of nitrogen fertilizer to the soil mitigated the water consumption of Moso bamboo and reduced sap flow rates. Peng [15] employed deep learning to model sap flow based on environmental parameters, highlighting light intensity and air and soil temperature as major predictive factors. In their model, the prediction of sap flow achieved an R^2 of 0.78, indicating moderate explanatory power. While these studies provide important insights, they have a fundamental limitation: Correlation does not imply causation. For instance, illumination intensity and sap flow may show high correlation (e.g., >0.9), but this does not indicate a direct or delayed causal link, nor reveal the direction of influence.

Most existing studies on sap flow focus on correlation analysis with environmental factors. However, correlation does not imply causation; it reflects only statistical association and cannot determine whether one variable causes changes in another [16]. Confounding variables and multicollinearity can further obscure the true relationships. Causal inference methods help address these limitations by revealing true causal mechanisms and accounting for biases in observational data. Researchers develop various frameworks, including the potential outcome framework and the structural causal model (SCM). SCM [17] is a popular framework for causal inference that unifies the strong features of structural equation modeling [18], Rubin's potential outcome framework [19], Bayesian network [20], among others, to create a robust causal relationship theory and inference framework. By fitting different structures, which are proposed based on prior knowledge of the current system, the inference process is completed. The final results are visualized in the form of graphs. SCM is currently widely used in various fields such as ecology [21], clinical medicine [22], and computer science [23,24].

Depending on the characteristics of the observational data, causal relationship discovery methods can be classified into those based on temporal and non-temporal observations. For non-temporal observational data, Liu [25] proposed the CASTLE (Causality Analysis model based on Structure Learning) method, which integrates information entropy from medical and biological aspects to identify molecular factors underlying drug adverse reactions. Wang [26] introduced a method that combines clustering with Bayesian network structure learning and applied it to traditional Chinese medicine research on kidney diseases. Zhou [27] proposed two novel causal algorithms for effective inference of large-scale cellular networks from noisy steady-state experimental data. For temporal observational data, Arif [21] applied the backdoor and front-door criteria from the SCM framework to determine causal relationships in observed ecosystem data and constructed visual DAGs, albeit with some limitations regarding confounding factors. Legnani [28] proposed the information causal entropy-complexity method to study changes in wall thickness and ventricular pressure dynamics in ischemic wall behavior systems, providing an objective indicator for the recovery of myocardial behavior after oxygen supply to the ventricular wall. Contreras-Reyes [29] utilized frequency domain Granger causality analysis and statistical significance testing to demonstrate that anomalies in the Pacific Decadal Oscillation and other regional changes are the main driving factors for variations in anchovy reproduction and indicators of physical condition.

Most researchers have focused on observational statistical analysis, but lacked in-depth investigation of causal relationships, and the results were not intuitive. In this study, the analysis based on causal inference can provide a deeper understanding of the relationship between sap flow and environmental factors in Moso bamboo. The major contributions of this paper are as follows: We construct a hybrid causal inference pipeline that integrates non-temporal (FCI) and temporal Latent

Peter-Clark Momentary Conditional Independence (LPCMCI) methods to study Moso bamboo sap flow; we identify meaningful causal links among factors with low correlation coefficients, demonstrating the inadequacy of traditional correlation methods; we quantify time-lagged causal effects and identify physiological implications (e.g., 80-minute lag for illumination effects); and we build a visualized framework for interpreting the complex dynamics between environmental variables and sap flow in natural bamboo forests.

2. Materials and methods

2.1. Experimental dataset

The data were collected from December 2019 to June 2021 at the Bamboo Experimental Forest in Jing County, Anhui Province. The study area is primarily composed of pure Moso bamboo (Phyllostachys edulis) forests with high canopy coverage. The soil is predominantly acidic red, and the hydrothermal conditions and soil characteristics are similar to those of major Moso bamboo-producing regions such as Anji in Zhejiang and Nanping in Fujian. However, they differ from marginal distribution areas such as the Sichuan Basin, which has a lower annual average temperature, and some regions in South China, which experience more pronounced seasonal rainfall [30]. Environmental factors were monitored using sensors [31], as shown in Figure 1(a). Specifically, the air temperature and relative humidity were measured using the HOBO U23 Pro v2 sensor (Onset Computer Corporation, USA), with an accuracy of ±0.2 °C for temperature and ±2.5% for relative humidity. Photosynthetically active radiation (PAR) was measured using an Apogee quantum sensor (SQ-500, Apogee Instruments Inc., USA; accuracy: ±5%). CO_2 concentration was monitored using a SenseAir S8 sensor (accuracy: ±50 ppm ±3% of reading). Soil moisture and soil temperature were measured using a Decagon 5TE sensor (METER Group, USA), with an accuracy of ±3% for volumetric water content and ±1 °C for temperature.

(a) (b)

Figure 1. Monitoring of environmental factors and sap flow density.

While variations in sap flow (SF, g/m2/s) of eight bamboo plants were monitored at the same location using a self-developed portable Moso bamboo sap flow monitor [32], the device is based on the heat-balance method, where a constant power is applied to a heating element inserted into the bamboo culm, and the resulting temperature gradient between upstream and downstream thermocouples is used to estimate sap flux density. The sensor includes three vertically aligned probes (one heater probe and two temperature probes) and is powered by a constant current source. The measurement accuracy is ±10% under standard conditions, and the resolution is 0.1 g/m²/s. The process

of installing the sap flow monitor on Moso bamboo is illustrated in Figure 1(b). First, holes were drilled into the bamboo using a drill bit, and heat-conducting gel was injected carefully without piercing through the bamboo wall. Subsequently, protective covers and waterproof tapes were added to prevent rainwater interference during detection. Finally, an additional layer of protective film was applied to prevent moisture from the air from damaging the equipment.

The collected sap flow and environmental factor data were stored and processed using the accompanying Internet of Things (IoT) system. The main environmental factors collected include air temperature (AT, ℃), air humidity (AH, %RH), soil temperature (ST, ℃), soil moisture (SM, %RH), illumination intensity (II, lux), and carbon dioxide concentration in the air (CO2C, ppm), with data collected every 10 minutes. We selected data from November 2020 to January 2021. To ensure data accuracy and the reliability of subsequent modeling, missing and abnormal values caused by equipment failures, sensor malfunctions, or human interference were first removed. Abnormality detection was primarily performed using a sliding window approach combined with the three-sigma rule (3σ) [33]. Then, linear interpolation was applied to fill in minor missing values, ensuring the continuity of the time series. To eliminate the impact of differing dimensions and value ranges among environmental factors and sap flow data, all variables were normalized to the [0, 1] interval using min-max scaling, facilitating subsequent analysis and model training. Due to the similar trends in sap flow density among the 8 bamboo plants in response to environmental changes, we plotted the sap flow density variations of 3 representative plants for clarity and better visualization. After normalization, the data are presented in Figure 2, where the horizontal axis represents time and the vertical axis represents the normalized distribution.

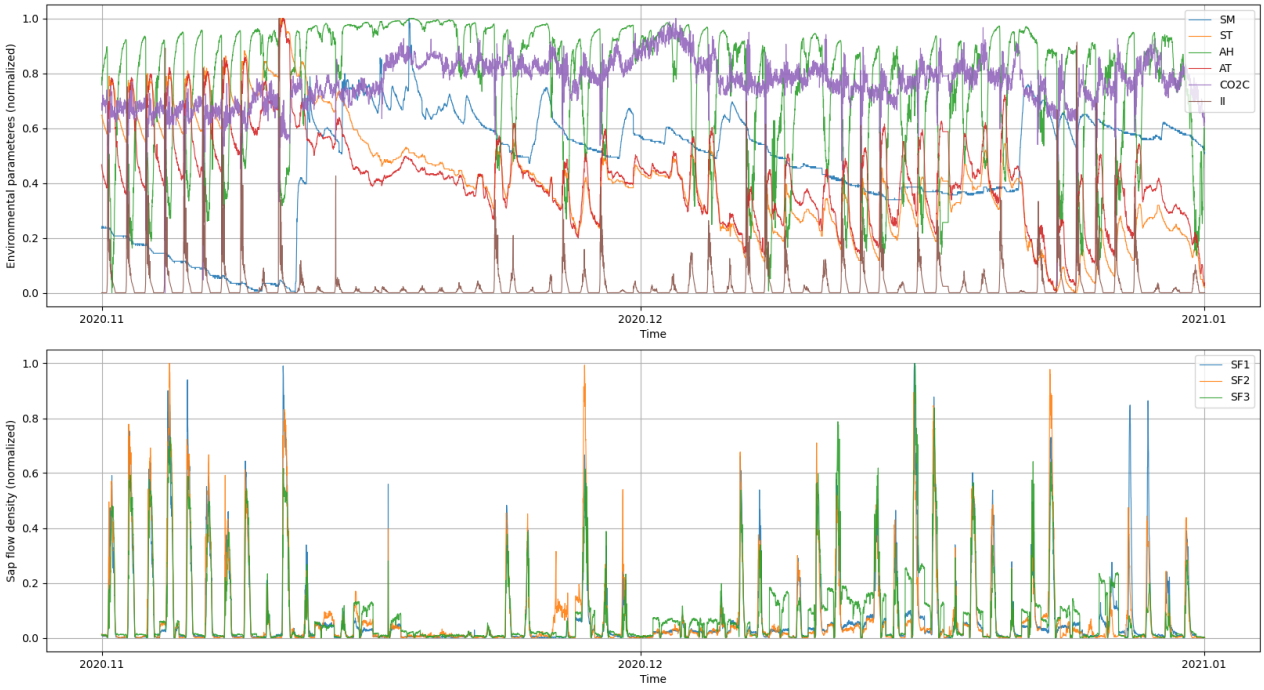

Figure 2. Data of bamboo forest environmental factors and bamboo SAP flow collected synchronously.

2.2. Grey relational analysis

We first conducted correlation analyses between Moso bamboo sap flow and environmental

factors to explore the correlation between variables and observe the limitations of correlation analysis methods. Grey relational analysis is a highly active branch of grey system theory, the main idea of which is to judge the closeness of the relationship between different sequences by analyzing the similarity of the geometric shapes of the sequence curves. The major steps are as follows [34]:

Step 1: Determining the system characteristic parameter sequence (sap flow) and the comparative sequence affecting the system (environmental factors).

Step2：Normalizing the reference and comparative sequences.

Step3：Calculating the grey relational coefficient ξ between the reference and the comparative sequence.

$$\xi_{0i}(j) = \frac{\min\limits_{i}\min\limits_{j}|x_0(j) - x_i(j)| + \rho\max\limits_{i}\max\limits_{j}|x_0(j) - x_i(j)|}{|x_0(j) - x_i(j)| + \rho\max\limits_{i}\max\limits_{j}|x_0(j) - x_i(j)|}, \tag{1}$$

ξ_{0i} denotes the grey relational coefficient between the reference sequence X_0 and the comparative sequence X_i, where ρ denotes the Dynamic Distinguishing Coefficient, generally ranging from 0 to 1, and j denotes the serial number.

Step4：Calculating correlation γ_i

ξ denotes the degree of correlation between the comparative and reference sequence at each moment; the information is too scattered. γ_i is the average value of the correlation coefficient.

$$\gamma_i = \frac{1}{N}\sum_{j=1}^{N}\xi_i(j), \tag{2}$$

Step5：Ranking correlation

Describing the relationship between factors by the order of the degree of correlation than just the magnitude. Finally, these correlation sequences are represented as a correlation matrix to observe the correlation between factors.

2.3. Causal inference

Correlation analysis primarily focuses on describing the relationship between variables than deriving cause-and-effect relationships. In contrast, causal inference methods focus on identifying true causal mechanisms by controlling for confounders. Given the complex relationship between Moso bamboo sap flow and environmental factors, correlation analysis alone is insufficient. Therefore, introducing causal inference offers a more scientific approach. Depending on data characteristics, causal methods can be divided into non-temporal and temporal approaches. The former uncovers overall structural relationships, while the latter captures time-lagged causal effects. We integrated both to comprehensively analyze the drivers of sap flow in Moso bamboo.

2.3.1. Causal inference based on non-temporal observation

There are several ways to represent causal graphs based on non-time-series data, mainly divided into three categories: Directed Acyclic Graph (DAG), Mixed Ancestral Graph [35] (MAG), and Partial Ancestral Graph [36] (PAG). Within the causal inference framework, DAGs are commonly used to represent the hypothesis of the causal structure of the research system or process [17,37]. The directed edges between variables represent the possibility of causal effects [38]. However, causal inference

algorithms based on DAG often result in a Markov equivalence class, as shown in Figure 3. They all satisfy the same d-separation property, where given a variable Z, variables X and Y are independent, written as $X \perp Y|Z$. This cannot accurately reflect the causal relationship between variables in real-world scenarios.

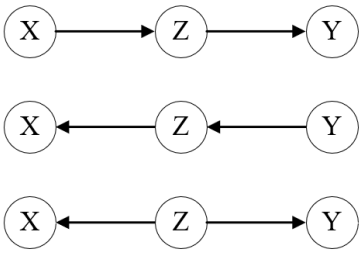

Figure 3. V-shaped structure of Markov equivalence.

MAG introduces an additional bidirectional edge $\leftrightarrow$ to denote potential confounding factors, which can indicate the uncertainty of the causal structure in DAG. For a set of equivalent DAGs corresponding to Figure 3, it can be represented simply in MAG as $X \leftrightarrow Y$. In causal inference, it is often desirable to express a set of assumed MAGs in a more concise manner, leading to the introduction of PAG. PAG can represent equivalence classes of MAG, providing a more concise representation and richer node representation methods. The causal structures expressed by PAGs often better meet the real-world scenarios. Connections between variables can be mainly classified into four types in a causal graph, as shown in Table 1.

Table 1. Relationships denoted by different connections in causal graph.

Connection Way	Relationships	Absent Relationships
A → B	A is the cause of B	B is not the cause of A
A ○→ B	A is the cause of B, or There is an unmeasured confounder between A and B	B is not the cause of A
A ↔ B	There is an unmeasured confounder between A and B	A is the cause of B B is the cause of A
A ○—○ B	One of the following five cases 1. A is the cause of B 2. B is the cause of A 3. There is an unmeasured confounder between A and B 4. Both 1 and 3 5. Both 2 and 3	NULL

Researchers have proposed numerous methods for non-temporal causal structure discovery, which can be broadly categorized into three types: constraint-based methods, score-based methods, and function-based modeling methods. Constraint-based methods offer high computational efficiency but rely on the causal sufficiency assumption, which is often difficult to meet in real-world applications. Score-based methods can generate multiple DAGs, but the number of possible graphs grows exponentially with the number of observed variables, making them impractical in large-scale settings. Function-based modeling approaches exhibit strong theoretical identifiability but typically assume linear or additive relationships, which are unsuitable for complex nonlinear and multi-path mechanisms, such as the feedback loops common in ecological systems.

FCI [39] is a constraint-based algorithm that does not require the causal sufficiency assumption and can account for latent confounders. It infers PAGs that better reflect real-world causal uncertainty. Moreover, it maintains good computational efficiency in high-dimensional scenarios and can be integrated with time-series frameworks as a structural prior, providing guidance for subsequent temporal causal analysis (e.g., LPCMCI).

2.3.2. Causal inference based on temporal observation

Temporal causal graphs extend DAGs by incorporating a time dimension, enabling the observation of causal relationships across time lags. As shown in Fig 4, they are typically categorized into three types: The full-time causal graph, the window causal graph, and the summary causal graph. Full-time causal graph offers detailed insights but are difficult to obtain in practice. A summary causal graph merely presents an overview of causal relationships, similar to standard DAGs, and can be derived from a window graph. The window causal graphs are a commonly used representation that reflects variable relationships within a certain lag time.

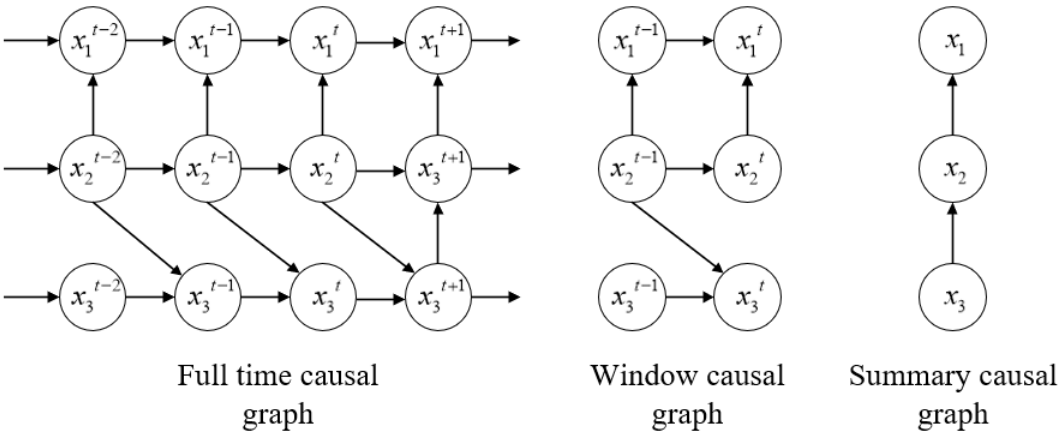

Figure 4. Different causal graphs extrapolated from the temporal data.

LPCMCI [40] is a causal inference algorithm for time series analysis, based on the Peter-Clark Momentary Conditional Independence PCMCI ([41] improved framework, which weakens the variable's self-dependence and improves the overall statistical effect, which does not need to meet the causal sufficiency assumption. Compared to FCI, LPCMCI focuses more on capturing time-lagged causal relationships, making it better suited for analyzing the dynamic response between Moso bamboo sap flow and environmental factors. It is also highly flexible, enabling integration with various

independence tests to accommodate different data types (continuous or discrete) and dependency structures (linear or nonlinear).

Additionally, the algorithm entails several parameters. The maximum considered time lag, denoted as τ_{max}, determines the observation time window $[t-\tau_{max}]$. Typically, τ_{max} is determined by assessing non-conditioned lagged dependencies in the observed data, selecting the lag with the maximum absolute dependency coefficient as τ_{max}. The significance threshold α_{PC} for individual independence testing. A larger α_{PC} yields denser temporal causal graphs. The number of iterations, denoted as k, typically set to 1 by default. The algorithm returns three main outputs: The graph (indicating connections between nodes), the p matrix (edges exist if p < α_{PC}), and the val matrix (representing the strength of the causal links).

3. Experiments and results

3.1. Experimental framework

Experiment flow is shown in Figure 5. Preliminary correlation analysis was conducted to explore statistical associations, after which its limitations, such as spurious correlation and confounding, are discussed. The FCI algorithm was applied for non-temporal causal discovery, generating a PAG. Subsequently, the LPCMCI algorithm was used to identify time-lagged causal relationships in the temporal domain. Finally, the results were interpreted, visualized, and summarized to support data-driven decision-making in bamboo ecological management.

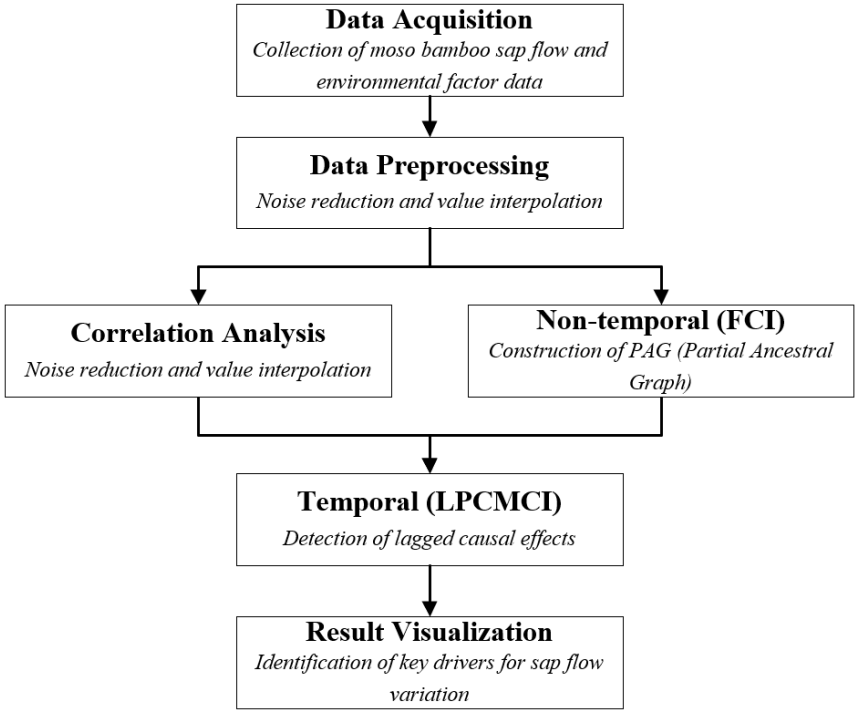

Figure 5. Experimental workflow chart.

3.2. Correlation analysis based on gray correlation

Using gray correlation to analyze the correlation between environmental factors and sap flow of Moso bamboo, results in a grey relational matrix, as shown in Fig. 6. Here, the closer the value in the matrix is to 1, the greater the correlation between the factors.

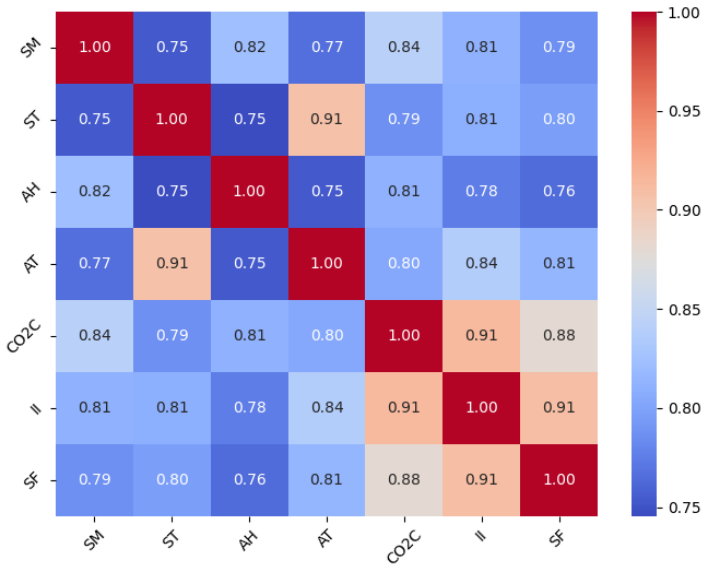

Figure 6. Gray correlation matrix between environmental factors and sap flow (SM: soil moisture, ST: soil temperature, AH: air humidity, AT: air temperature, CO2C: carbon dioxide concentration, II: illumination intensity, and SF: sap flow density).

Figure 6 shows strong correlations among several factors, with II, CO2C, and AT exhibiting correlation coefficients above 0.8. However, the causal relationships and effects between these factors cannot be inferred from the correlation matrix alone. For instance, it is unclear from the correlation matrix whether the CO2C promotes or inhibits SF, and whether there exists a causal relationship between them. Therefore, the correlation matrix may not provide intuitive insights. In the face of larger environmental systems or other data analyses, correlations may lead to disturbances in decision-making and result in erroneous interpretations.

3.3. Causal discovery based on the distribution of data

We utilized the FCI algorithm for causal inference between the environmental factors and Moso bamboo sap flow [42]. Thereafter, we combined this with expert, prior knowledge to obtain the PAG shown in Figure 7.

For the characteristics of bamboo sap flow, the major influencing factors are ST, SM, CO2C, and AH. The causal relationship between AH and SF can be explained from the perspective of plant transpiration. AH, to some extent, affects the evaporation of water from bamboo leaves, thereby influencing the SF [43]. The causal relationship between CO2C, ST, and SF is bidirectional. From the perspective of plant root respiration, changes in ST affect root respiration and microbial activity in the soil, including the decomposition of organic matter, leading to the exchange of CO2C between soil and air. These changes also affect bamboo's physiological activities, thus influencing SF [44].

Additionally, it is conceivable that other factors may influence photosynthetic rate, thereby affecting the SF and CO2C [45].

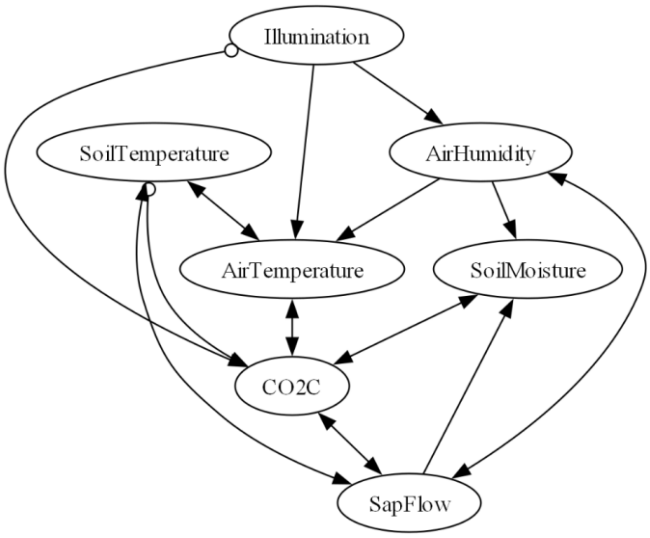

Figure 7. Non-temporal causal relationships between environmental factors and sap flow.

Comparing Figures 6 and 7, we observe that the correlation coefficients between AT and ST, as well as between II and CO2C, both reach 0.91. Correspondingly, these relationships are reflected in PAG with the respective causal connections. However, while the correlation coefficient between SF and II also reaches 0.91, there is no apparent causal relationship in the PAG. Moreover, based on common knowledge, changes in II can influence ST. However, this causal relationship is not evident in the PAG. This analysis suggests that FCI may not effectively consider causal relationships in the temporal dimension. For better visualization and intuitive observation, we plotted the data for ST, II, and SF for the first 1500 sampling instances, as depicted in Figure 8.

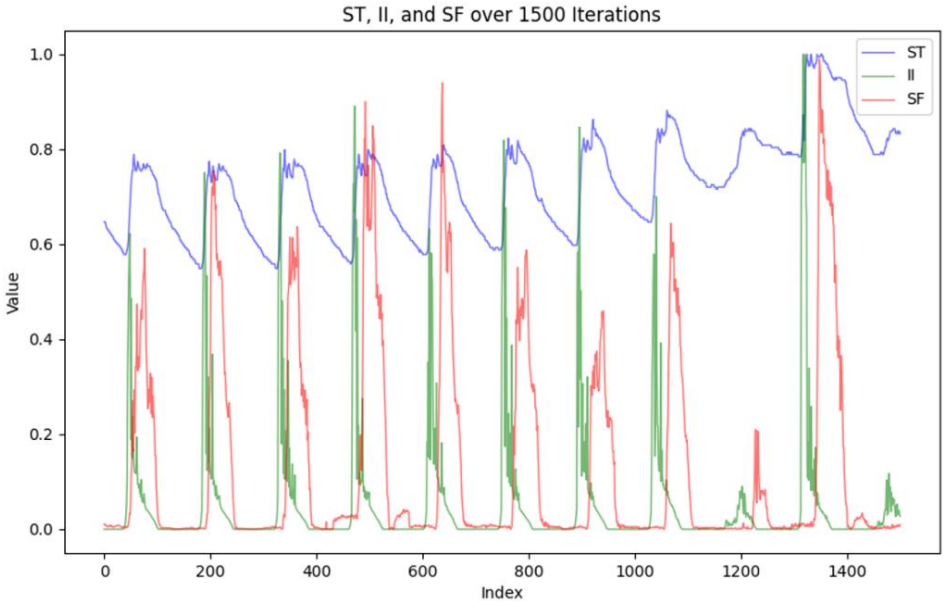

Figure 8. Variation in time-series data of sap flow, light intensity, and soil temperature.

Figure 8 shows that the changes of SF and ST have a certain time lag with the changes of II, and the effects caused by II need time before they can be transferred to other environmental factors. We need to further analyze the temporal causal relationship between different factors.

3.4. Temporal causal discovery

In order to select an appropriate τ_{max}, we plotted a scatter plot τ with the lagged dependence, from which we intercepted the lagged dependence between sap flow and other environmental factors, as shown in Figure 9.

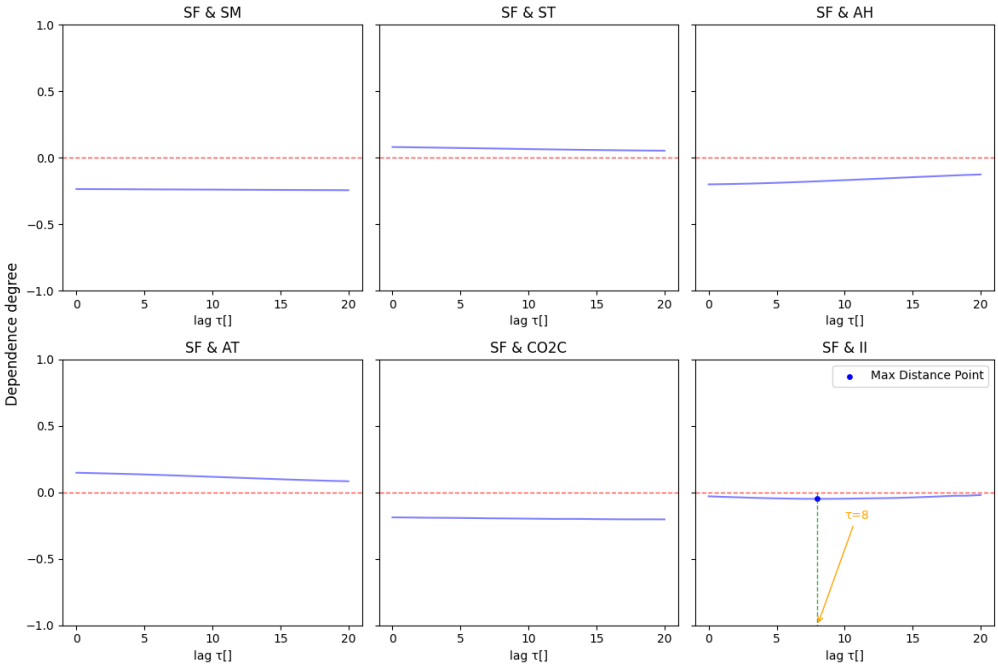

Figure 9. Lagged dependence between environmental factors and sap flow.

The horizontal axis represents τ, and the vertical axis denotes the corresponding lagged dependence. The dependence between SF and SM and CO2C remains relatively stable, while that with ST, AT, and AH gradually weakens over time. Notably, the dependence between II and SF first increases and then decreases, indicating a non-instantaneous, time-lagged correlation. To comprehensively capture the relationships between SF and all environmental factors. We choose $\tau_{max} = 8$. This choice balances the inference across variables while preserving the delayed relationship between SF and II.

The experiment sets $\tau_{max} = 8$ as the input parameter. The significance level α_{PC} is set to the default value of 0.1, and the number of iterations k is 30. The PAG inferred by FCI is used as prior knowledge for LPCMCI, and the resulting time-lagged causal graph between all factors and sap flow is shown in Figure 10. Each node represents an observed variable, with color intensity (from the auto-MCI bar) indicating self-dependence strength; red for positive and blue for negative effects. Directed edges represent dependencies as defined in Table 1, with arrow color reflecting the MCI strength. Numbers on edges denote the lag τ, where lower numbers indicate stronger dependence. For instance, the edge from illumination to SF marked with τ = 8 implies that increased II enhances SF after

approximately 1 hour (given a 10-minute sampling interval). Similarly, II influences ST after a lag of about 40 minutes.

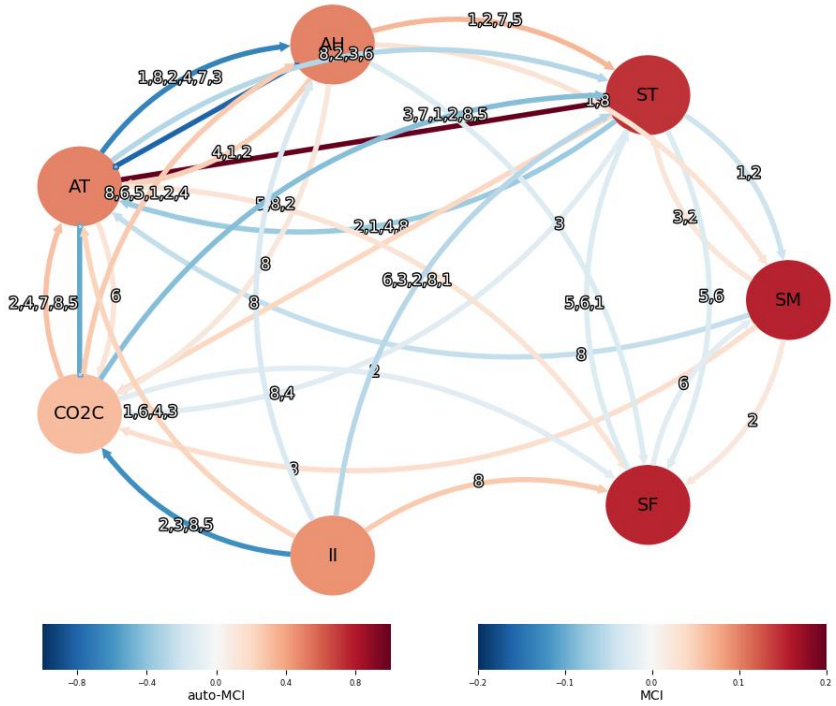

Figure 10. Temporal causality between environmental factors and sap flow.

We focus on the causal relationships between environmental factors and sap flow. The resulting p_matrix is shown in Table 2, where each column represents the maximum p-value from all conditional independence tests between an environmental factor and SF. A higher p-value indicates a greater likelihood of independence. As shown in Table 2, the p-value between SM and SF at lag $\tau = 2$ is below the significance threshold α_{PC}, suggesting a likely association. Similarly, significant associations are observed for ST at $\tau = 5$ and 6, AH at $\tau = 3$, AT at $\tau = 2$, 5, and 8, CO2C at $\tau = 2$, and II at $\tau = 8$. The remaining p-values exceed the significance level α_{PC}, indicating insufficient evidence to reject the null hypothesis; in other words, these variables are considered independent with no associated edges. Simply, only p-values below the threshold suggest the presence of a causal link.

Table 2. P-values of the conditional independence test under different lags.

P-value	$\tau = 0$	$\tau = 1$	$\tau = 2$	$\tau = 3$	$\tau = 4$	$\tau = 5$	$\tau = 6$	$\tau = 7$	$\tau = 8$
SM	0.550	0.712	**0.062**	0.107	0.267	0.125	0.345	0.934	0.327
ST	0.178	0.558	0.617	0.158	0.486	**0.013**	**0.019**	0.269	0.507
AH	0.750	0.873	0.279	**0.047**	0.493	0.244	0.598	0.410	0.104
AT	0.696	0.327	**0.098**	0.359	0.474	**0.012**	0.917	0.701	**0.027**
CO2C	0.357	0.684	**0.053**	0.997	0.568	0.950	0.788	0.508	0.607
II	0.454	0.302	0.735	0.754	0.265	0.543	0.737	0.721	**0.000**

Figure 10 presents a comprehensive and complex temporal causal graph. However, since our focus of this study is on sap flow variation in relation to Moso bamboo growth and how environmental factors influence it, we concentrate on the causal analysis of sap flow. Edges unrelated to sap flow are therefore masked, resulting in the sap flow-centered temporal causal graph shown in Figure 11.

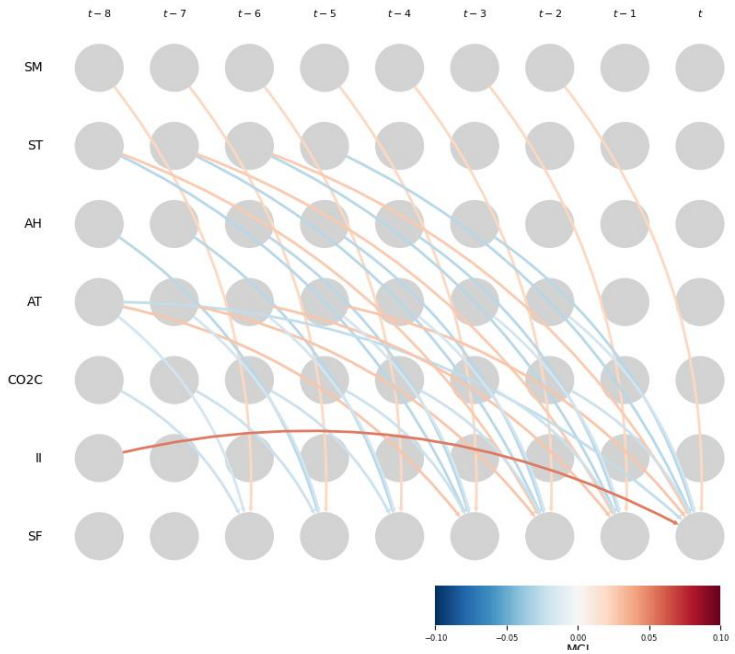

Figure 11. Windowed causal graph of the effects of environmental factors on sap flow.

As shown in Figure 11, the effect of SM on SF exhibits a lag of 20 minutes, indicating that Moso bamboo begins to enhance water uptake after a delay, with moderate SM playing a promoting role in SF. The lag between II and SF is longer, around 80 minutes, which is consistent with previous findings [46,47] that the time-lag effect of light radiation on plant sap flow is approximately one hour. This is mainly because increased II stimulates stomatal opening, leading to enhanced transpiration and thus greater water consumption. Elevated CO2C appears to suppress SF, as stomata, the primary channels for transpiration, tend to close or reduce aperture under high CO2C conditions [48]. This reduces the transpiration rate, lowers the root water uptake demand, and subsequently decreases SF. AH also shows a suppressive relationship with SF, which can be explained by transpiration dynamics: In high-humidity environments, the actual vapor pressure approaches saturation, hindering the phase transition from liquid to vapor, thus reducing evaporation efficiency [49].

Due to the complexity of environmental systems, the effects of ST and AT on SF vary at different lag times, showing an overall trend of initial suppression followed by promotion. This may be because early temperature changes trigger water regulation mechanisms that temporarily reduce SF. Over time, as plants adapt to temperature changes, root water uptake and SF gradually recover and exceed the initial level, resulting in a net promoting effect.

4. Discussion

We systematically investigated the influence of environmental factors on Moso bamboo sap flow density using correlation analysis and causal inference methods. Compared with traditional

correlation-based approaches, the integration of FCI and LPCMCI algorithms offers greater interpretability in identifying potential causal pathways. Although AT showed low correlation with SF, the PAG structure constructed by FCI revealed potential causal links, suggesting that weakly correlated factors may have significant causal effects. The time-lagged causal graph obtained via LPCMCI further illustrated the delayed effects of different factors: High CO2C, dry soil, and AH had short-term inhibitory effects on SF, while increased light and temperature showed longer-term promoting effects.

However, the study has certain limitations. The limited number of monitoring points may not fully capture individual variability within the bamboo population. Additionally, the robustness of the causal framework under high-dimensional data or hidden confounders requires further validation. Future research will extend the observation period to a full-year scale, incorporate additional physiological indicators, and develop a more robust causal model. This aims to enable the prediction of bamboo physiological states based on environmental conditions, providing a theoretical foundation and technical support for forest management and ecological response studies.

Use of AI tools declaration

The authors declare they have not used Artificial Intelligence (AI) tools in the creation of this article.

Acknowledgments

This work was supported by Forestry Science and Technology Extension Demonstration Project (hx23350), the National Key Research and Development Program (2018YFD0600101).

Conflict of interest

The authors declare there is no conflict of interest.

References

1. Z. Zheng, N. Yan, Z. Lou, X. Jiang, X. Zhang, S. Chen, et al., Modification and application of bamboo-based materials: a review—Part II: application of bamboo-based materials, *Forests,* **14** (2023), 2266. https://doi.org/10.3390/f14112219
2. M. Zhang, S. Chen, H. Jiang, Y. Lin, J. Zhang, X. Song, et al., Water-use characteristics and physiological response of moso bamboo to flash droughts, *Int. J. Environ. Res. Public Health,* **16** (2019), 2174. https://doi.org/10.3390/ijerph16122174
3. J. Li, L. Chen, J. Wang, J. Xu, H. Zheng, Y. Bai, et al., Spatiotemporal dynamic changes in transpiration in the shoot sheath and its relation to water transportation during rapid growth of Moso bamboo, *Front. Forests Global Change,* **7** (2024), 1343206. https://doi.org/10.3389/ffgc.2024.1343206
4. K. H. Jensen, K. Berg-Sørensen, H. Bruus, N. M. Holbrook, J. Liesche, A. Schulz, et al., Sap flow and sugar transport in plants, *Rev. Modern Phys.,* **88** (2016), 035007. https://doi.org/10.1103/RevModPhys.88.035007
5. M. A. Forster, How significant is nocturnal sap flow? *Tree Physiol.,* **34** (2014), 757–765. https://doi.org/10.1093/treephys/tpu051

6. Y. Li, L. Guo, J. Wang, Y. Wang, D. Xu, J. Wen, An improved sap flow prediction model based on CNN-GRU-BiLSTM and factor analysis of historical environmental variables, *Forests,* **14** (2023), 1310. https://doi.org/10.3390/f14071310
7. L. Zhu, J. Xu, Y. Zhang, P. Luo, Z. Shi, J. Hou, et al., Analysis on diurnal variation of sap flow in Pinus massoniana and its influencing factors in Luoyang, Henan Province, China, *J. Nanjing Forest. Univer.,* **47** (2023), 92. https://doi.org/10.12302/j.issn.1000-2006.202106005
8. M. Li, H. Dang, S. Chen, C. Liiu, W. Yang, Y. Qiao, Sap flow variation in Pinus sylvestris var. mongolica plantation at the southern margin of Mu Us sandy land and its response to environmental factors, *J. Arid Land Resources Environ.,* **37** (2023), 153–161. https://doi.org/10.13448/j.cnki.jalre.2023.098
9. C. Tong, X. Zhang, J. Xie, T. Mei, D. Fang, Y. Li, Water use strategies of different aged moso bamboo culms under summer drought, *Forest Ecol. Manag.,* **498** (2021), 119567. https://doi.org/10.1016/j.foreco.2021.119567
10. B. Fan, Z. Liu, K. Xiong, Y. Li, K. Li, X. Yu, Influence of environmental factors on the sap flow activity of the golden pear in the growth period of karst area in southern China, *Water,* **14** (2022), 1707. https://doi.org/10.3390/w14111707
11. X. Hou, J. Xie, R. Ge, Phyllostachys pubescens sap flow and its relationships with environm ental factors, *Chinese J. Ecol.,* **29** (2010), 1263–1269. https://doi.org/10.13292/j.1000-4890.2010.0224
12. D. Gu, W. He, K. Huang, D. Otieno, C. Zhou, C. He, et al., Transpiration of Moso bamboo in southern China is influenced by ramet age, phenology, and drought, *Forest Ecol. Manag.*, **450** (2019), 117526. https://doi.org/10.1016/j.foreco.2019.117526
13. X. Liu, D. Xie, J. Zhang, J. Zhuang, Q. Shi, J. Yue, et al., A study on water consumption characteristics of Phyllostachys edulis, a typical afforestation species in Southern Jiangsu Province of China, *J. Nanchang Institute Technol.,* **33** (2014), 16–22.
14. X. Wu, S. Liu, J. Luan, Y. Wang, X. Gao, C. Chen, Nitrogen addition alleviates drought effects on water status and growth of Moso bamboo (Phllostachys edulis), *Forest Ecol. Manag.,* **530** (2023), 120768. https://doi.org/10.1016/j.foreco.2023.120768
15. S. Peng, W. Jia, P. Deng, Z. Jiang, Prediction of Moso bamboo sap flow based on environmental parameters and deep learning models, *Transact. Chinese Soc. Agri. Eng. (Transact. CSAE),* **41** (2025), 201–208. https://doi.org/10.11975/j.issn.1002-6819.202407229
16. M. Van Hul, T. Le Roy, E. Prifti, M. C. Dao, A. Paquot, J.-D. Zucker, et al., From correlation to causality: The case of Subdoligranulum, *Gut Microbes,* **12** (2020), 1–13. https://doi.org/10.1080/19490976.2020.1849998
17. J. Pearl, Causality: Models, Reasoning and Inference, 2nd ed, New York: Cambridge university press, 2003, 675–685p. https://doi.org/10.1017/S0266466603004109
18. B. Shipley, Cause and correlation in biology: A user's guide to path analysis, structural equations and causal inference with R, 2nd ed, New York: Cambridge university press, 2016, 353p. https://doi.org/10.1017/CBO9781139979573
19. D. B. Rubin, Causal inference using potential outcomes: Design, modeling, decisions, *J. Am. Statist. Assoc.,* **100** (2005), 322–331. https://doi.org/10.1198/016214504000001880
20. M. R. Waldmann, L. Martignon, A Bayesian network model of causal learning, *Proceedings of the twentieth annual conference of the Cognitive Science Society*, Madison, WI, USA, Mahwah (NJ): Lawrence Erlbaum Associates, 1998, 1102–1107p.
21. S. Arif, M. A. MacNeil, Applying the structural causal model framework for observational causal

inference in ecology, *Ecol. Monographs,* **93** (2023), e1554. https://doi.org/10.1002/ecm.1554
22. M. O. Gani, S. Kethireddy, R. Adib, U. Hasan, P. Griffin, M. Adibuzzaman, Structural causal model with expert augmented knowledge to estimate the effect of oxygen therapy on mortality in the icu, *Artific. Intell. Med.,* **137** (2023), 102493. https://doi.org/10.1016/j.artmed.2023.102493
23. A. Geiger, Z. Wu, H. Lu, J. Rozner, E. Kreiss, T. Icard, et al., Inducing causal structure for interpretable neural networks, *International Conference on Machine Learning*, Baltimore, MD, USA, Proceedings of Machine Learning Research, PMLR, 2022, 7324–7338p.
24. Y. Wang, S. He, Q. Luo, H. Yuan, L. Zhao, J. Zhu, et al., Causal invariant geographic network representations with feature and structural distribution shifts, *Future Gener. Comput. Syst.,* **169** (2025), 107814. https://doi.org/10.1016/j.future.2025.107814
25. M. Liu, R. Cai, Y. Hu, M. E. Matheny, J. Sun, J. Hu, et al., Determining molecular predictors of adverse drug reactions with causality analysis based on structure learning, *J. Am. Med. Inform. Assoc.,* **21** (2014), 245–251. https://doi.org/10.1136/amiajnl-2013-002051
26. M. Wang, Z. Geng, M. Wang, F. Chen, W. Ding, M. Liu, Combination of network construction and cluster analysis and its application to traditional Chinese medicine, *Advances in Neural Networks-ISNN 2006: Third International Symposium on Neural Networks, Chengdu, China, May 28-June 1, 2006, Proceedings, Part III 3*, Springer, 777–785.
27. T. Zhou, Y. Wang, Causal relationship inference for a large-scale cellular network, *Bioinformatics,* **26** (2010), 2020–2028. https://doi.org/10.1093/bioinformatics/btq325
28. W. Legnani, F. Traversaro, F. O. Redelico, L. J. Cymberknop, R. L. Armentano, O. A. Rosso, Analysis of ischaemic crisis using the informational causal entropy-complexity plane, *Chaos,* **28** (2018), 075518. https://doi.org/10.1063/1.5026422
29. J. E. Contreras-Reyes, C. Hernández-Santoro, Assessing Granger-causality in the southern Humboldt current ecosystem using cross-spectral methods, *Entropy,* **22** (2020), 1071. https://doi.org/10.3390/e22101071
30. M. Xu, H. Ji, S. Zhuang, Carbon stock of Moso bamboo (Phyllostachys pubescens) forests along a latitude gradient in the subtropical region of China, *PloS One,* **13** (2018), e0193024. https://doi.org/10.1371/journal.pone.0193024
31. J. Zhang, Z. Jiang, B. Li, J. Gao, Internet of Things (IoT) system for environmental monitoring of bamboo forests, *Int. Thins Technol.,* **10** (2020), 19–23. https://doi.org/10.16667/j.issn.2095-1302.2020.01.005
32. J. Zhang, Z. Jiang, B. Li, W. Wu, J. Gao, Design and experiment of portable plant sap flow meter based on TDP, *Transact. Chinese Soc. Agri. Mach.,* **51** (2020), 237–243. https://doi.org/10.6041/j.issn.1000-1298.2020.07.027
33. L. L. Pauwels, A. L. Vasnev, A note on the estimation of optimal weights for density forecast combinations, *Int. J. Forecast.,* **32** (2016), 391–397. https://doi.org/10.1016/j.ijforecast.2015.09.002
34. S. A. Javed, A. Gunasekaran, A. Mahmoudi, DGRA: Multi-sourcing and supplier classification through Dynamic Grey Relational Analysis method, *Comput. Indust. Eng.,* **173** (2022), 108674. https://doi.org/10.1016/j.cie.2022.108674
35. T. S. Richardson, P. Spirtes, Ancestral graph Markov models, *Ann. Stat.,* **30** (2002), 962–1030. https://doi.org/10.1214/aos/1031689015
36. J. Zhang, Causal reasoning with ancestral graphs, *J. Mach. Learn. Res.,* **9** (2008), 1437–1474.
37. S. L. Morgan, C. Winship, Counterfactuals and the Potential Outcome Model, *Counterfactuals*

and Causal Inference: Methods and Principles for Social Research, 2nd ed, New York: Cambridge University Press, 2014, 37–76p.
38. F. Elwert, Graphical Causal Models, *Handbook of causal analysis for social research*, New York: Springer, 2013, 245–273p.
39. P. Spirtes, C. Glymour, R. Scheines, Causation, prediction, and search, 2nd ed, Cambridge: MIT press, 2001, 548p.
40. A. Gerhardus, J. Runge, High-recall causal discovery for autocorrelated time series with latent confounders, *Adv. Neural Inform. Process. Syst.,* **33** (2020), 12615–12625. https://doi.org/10.48550/arXiv.2007.01884
41. J. Runge, P. Nowack, M. Kretschmer, S. Flaxman, D. Sejdinovic, Detecting and quantifying causal associations in large nonlinear time series datasets, *Sci. Adv.,* **5** (2019), e4996. https://doi.org/10.1126/sciadv.aau4996
42. Y. Zheng, B. Huang, W. Chen, J. Ramsey, M. Gong, R. Cai, et al., Causal-learn: Causal Discovery in Python, arXiv preprint arXiv:230716405. https://doi.org/10.48550/arXiv.2307.16405
43. C. Ye, D. Hölscher, H. Du, F. Berninger, T. Mei, Partitioning of respired CO_2 in newly sprouted Moso bamboo culms, *Front. Plant Sci.,* **14** (2023), 1154232. https://doi.org/10.3389/fpls.2023.1154232
44. Y. Diao, X. Zheng, Y. Wang, Z. Xu, T. Song, D. Lang, et al., Effects of soil temperature and toisture on soil CO_2 concentration of wheat fields, *Climat. Environ. Res.,* **9** (2004), 584–590. https://doi.org/10.3878/j.issn.1006-9585.2004.04.04
45. R. Li, Y. He, J. Chen, S. Zheng, C. Zhuang, Research progress in improving photosynthetic efficiency, *Int. J. Molecular Sci.,* **24** (2023), 9286. https://doi.org/10.3390/ijms24119286
46. H. Wang, P. Zhao, X. Cai, L. Ma, X. Rao, X. Zeng, Time lag effect between stem sap flow and photosynthetically active radiation, vapor pressure deficit of Acacia mangium, *J. Appl. Ecol.,* **19** (2008), 225–230.
47. H. Wang, K. He, R. Li, Z. Sheng, Y. Tian, J. Wen, et al., Impact of time lags on diurnal estimates of canopy transpiration and canopy conductance from sap-flow measurements of Populus cathayana in the Qinghai–Tibetan Plateau, *J. Forest. Res.,* **28** (2017), 481–490. https://doi.org/10.1007/s11676-016-0333-z
48. A. Houshmandfar, G. J. Fitzgerald, M. Tausz, Elevated CO_2 decreases both transpiration flow and concentrations of Ca and Mg in the xylem sap of wheat, *J. Plant Physiol.,* **174** (2015), 157–160. https://doi.org/10.1016/j.jplph.2014.10.008
49. X. Gong, G. Lü, X. He, B. Sarkar, X. Yang, High air humidity causes atmospheric water absorption via assimilating branches in the deep-rooted tree Haloxylon ammodendron in an arid desert region of Northwest China, *Front. Plant Sci.,* **10** (2019), 573. https://doi.org/10.3389/fpls.2019.00573

AIMS Press